

Oxidative Stabilization of Dilute Ether Electrolytes via Anion Modification

John Holoubek, Qizhang Yan, Haodong Liu, Emma J. Hopkins, Zhaohui Wu, Sicen Yu, Jian Luo, Tod A. Pascal, Zheng Chen, and Ping Liu*



Cite This: *ACS Energy Lett.* 2022, 7, 675–682



Read Online

ACCESS |



Metrics & More

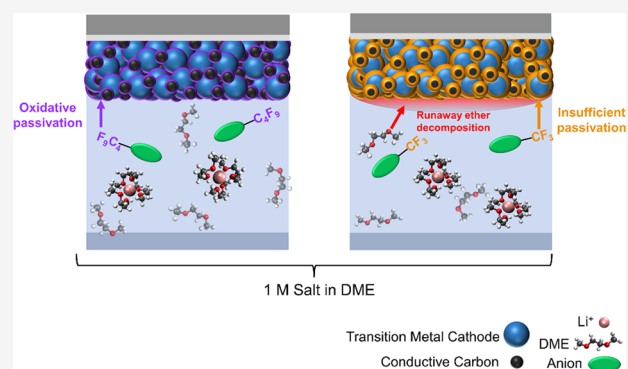


Article Recommendations



Supporting Information

ABSTRACT: State-of-the-art lithium metal batteries typically rely on ether electrolytes with high salt concentration and/or fluorinated solvents to enable stable cycling. Their high manufacturing costs at scale have motivated us to consider dilute, nonfluorinated ether electrolytes. However, their poor oxidative stability has precluded their application in cells employing transition-metal oxide cathodes, which operate at >4 V vs Li/Li⁺. Herein, we present a possible route forward for the oxidative stabilization of these electrolytes, which enabled the reversible cycling of LiNi_{0.8}Mn_{0.1}Co_{0.1}O₂ at a cutoff of 4.4 V in electrolytes composed only of 1 M salt and 1,2-dimethoxyethane. Through computational and experimental material characterization, it was determined that this behavior was driven by a passivating interphase composed largely of perfluoro alkane species. This work provides a method for the oxidative stabilization of ether electrolytes with a low base materials cost.



Lithium-ion batteries (LIBs) are approaching their theoretical maximum energy density at the cell level, necessitating a shift from the commercially dominant graphite anode (372 mAh g⁻¹) to Li metal (3860 mAh g⁻¹).¹ The typically employed electrolytes composed of carbonate solvents (e.g., ethylene carbonate, EC) have a tendency to undergo reductive decomposition, forming a solid-electrolyte interphase (SEI), which effectively protects the graphite anode from further parasitic reactions during repeated cycling.^{2,3} However, the same reactive electrolytes fail to stabilize Li metal due to the effectively infinite volume change associated with Li metal plating, which compromises the carbonate-derived SEI. Hence, carbonate-based electrolytes have a tendency to produce reduced Coulombic efficiency (CE), and dendritic growth during Li metal cycling which inevitably result in poor cycle life, and potential safety concerns due to cell shorting.^{4–6}

Ether solvents have a tendency to display substantially improved reductive stabilities when compared to carbonates, which have led to their application in emerging Li metal battery chemistries.^{2,6–12} However, the inherent reductive stability of ether solvents is not a result of a widened band gap, and instead is commensurate with a diminished oxidative stability. Functionally, it is well-documented that dilute ether electrolytes fail to support cathode chemistries at >4 V vs Li/Li⁺.^{13–15} This is particularly troublesome given that the commercially viable cathode chemistries capable of providing

the highest cell-level energy densities lie within this voltage range.¹ Increasing the salt concentration,^{9,13–15} and/or the introduction of fluorinated species,^{8,10,12,15} have been shown to extend the oxidative stability limit of ether electrolytes; however, the high cost of these components, relative to typical solvents, render this a suboptimal strategy.

The majority of state-of-the-art LMB electrolytes in the literature are formulated to provide optimal performance.^{8,16–18} While the upper limit of LMB performance, irrespective of cost, must be explored to achieve LMB commercialization, there is also the need to elucidate the performance limits of economically desirable systems. In this regard, strategies to improve the Li metal performance of dilute carbonate-based electrolytes through the addition of low-percentage electrolyte additives,¹⁹ 3-D hosts to facilitate uniform Li metal deposition,^{20–22} and Li metal electrode coatings^{23,24} have been demonstrated. However, extending the oxidative limits of low-cost ether systems is relatively under-addressed, which will be the focus of this work.

Received: December 14, 2021

Accepted: January 13, 2022

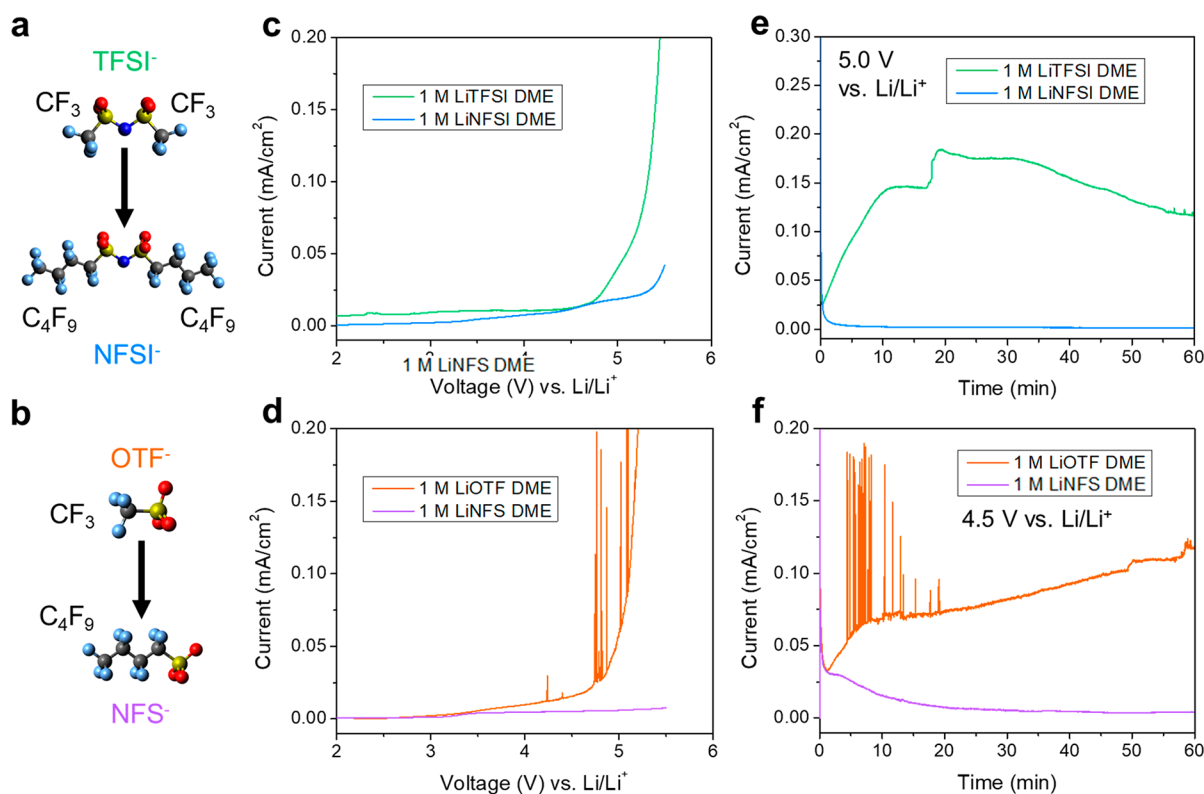


Figure 1. Molecular visualization of fluorocarbon chain length modification in (a) bis(C_xF_y sulfonyl)imide and (b) C_xF_y sulfonate moieties. Linear scan voltammetry profiles of Li||Al coin cells at 1 mV s^{-1} employing (c) 1 M LiTFSI and LiNFSI in DME and (d) 1 M LiOTF and LiNFS in DME. Potentiostatic profiles of Li||Al coin cells employing (e) 1 M LiTFSI and LiNFSI in DME at 5.0 V and (f) 1 M LiOTF and LiNFS in DME at 4.5 V.

Lithium bis(trifluoromethane sulfonyl)imide (TFSI) and trifluoromethanesulfonate (OTF) are common salts often paired with ether solvents, and have historically been applied in lithium–sulfur batteries, which typically do not exceed 3 V vs Li/Li⁺ during operation.^{25–28} However, ether electrolytes utilizing these salts are known to be incapable of operating above 4 V, which has limited use at dilute concentration.^{12,15} To examine the impact of anionic structure on these capabilities, we have chosen to examine lithium bis-(nonafluorobutane sulfonyl)imide (LiNFSI) and lithium nonafluorobutanesulfonate (LiNFS), which share the defining bis(C_xF_y sulfonyl)imide and C_xF_y sulfonate moieties with TFSI and OTF, respectively, but substitute the terminal CF_3 groups with C_4F_9 chains (see Figures 1a and 1b). Note that despite the current relatively high cost of these long-chain salts, their synthesis route is essentially identical to their CF_3 counterparts, which implies that the cost for their production would scale similarly given an increased market demand.²⁹ These salts were employed in the common nonfluorinated ether solvent, DME at 1 M to maintain an ostensibly low raw materials cost, as discussed previously.

As an initial indication of oxidative stability, linear-scan voltammetry was conducted on blank Al current collectors in order to determine the onset voltage and kinetic severity of the oxidative decomposition. As shown in Figure 1c, the onset of oxidative decomposition was found to be $\sim 4.8 \text{ V}$ vs Li/Li⁺ in 1 M LiTFSI DME, whereas 1 M LiNFSI DME was substantially extended to $\sim 5.3 \text{ V}$ vs Li/Li⁺. This trend of improved stability with extended C_xF_y chain length was also maintained in the sulfonate moiety, where the oxidative onset of 1 M LiOTF DME decomposition was observed at $\sim 4.7 \text{ V}$, as opposed to

$>5.5 \text{ V}$ in 1 M LiNFS (Figure 1d). In addition, the endowed stability of the long-chain anions was found to persist over extended time scales, where potentiostatic holds at 5.0 and 4.5 V vs Li/Li⁺ were found to produce progressive decomposition in 1 M LiTFSI and 1 M LiOTF DME, respectively, whereas the 1 M LiNFSI and 1 M LiNFS solutions produced negligible current responses under the same conditions as their CF_3 terminated counterparts (see Figures 1e and 1f). Also note that these trends are maintained when the Al blocking electrode is swapped with stainless steel, which is known to be more susceptible to corrosion in ether electrolyte systems (see Figure S1 in the Supporting Information).¹⁴

To understand how the oxidative stability trends gleaned from LSV apply to $>4 \text{ V}$ composite cathodes, a NMC 811:Super P:poly(vinylidene fluoride) (PVDF) mass ratio of 80:10:10 was employed in half cells and cycled at a cutoff of 4.4 V. As shown in Figure 2, the C_4F_9 anion variants showed substantial improvements of the cyclability of the applied cathodes when compared to their CF_3 counterparts. When considering the electrolytes containing sulfonylimide salts, the poor cycling of 1 M LiTFSI DME, which displayed 7.35 mAh g^{-1} after 26 cycles before encountering runaway decomposition (Figure 2a) was improved to 146 and 126 mAh g^{-1} after 50 and 100 cycles, respectively when replaced with LiNFSI (Figure 2b). On the other hand, 1 M LiOTF, which failed to produce a single reversible cycle (Figure 2c), was improved to 149 and 121 mAh g^{-1} after 50 and 100 cycles, respectively, when replaced with LiNFS (Figure 2d). Also note that the first discharge capacity varies significantly, which may be a direct result of altered charge-transfer kinetics or CEI chemistry between systems. The cycling profiles are shown in

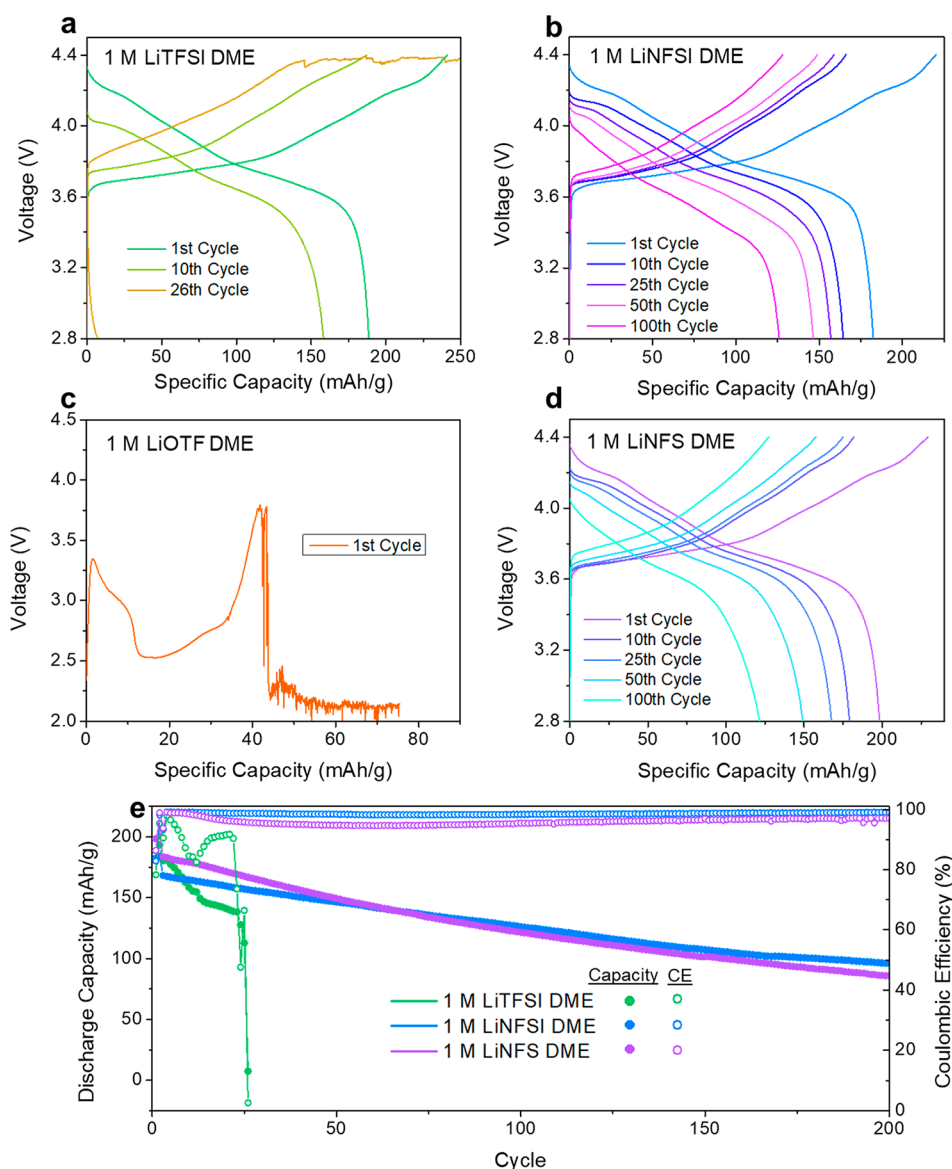


Figure 2. Galvanostatic cycling performance of Li|NMC 811 half cells with a 80:10:10 NMC:Super P:PVDF mass ratio and an active mass loading of $\sim 5 \text{ mg cm}^{-2}$. Voltage profiles of cells employing (a) 1 M LiTFSI DME, (b) 1 M LiNFSI DME, (c) 1 M LiOTF DME, and (d) 1 M LiNFS DME. (e) Long-term cycling performance of cells. All cells were charged to 4.4 V with two initial cycles at C/10, followed by C/3 cycling.

Figure 2e, where it is observed that the 1 M LiNFSI DME electrolyte offered a substantial improvement in both capacity retention and average Coulombic efficiency over all of the systems of interest.

When examining the voltage profiles of the aforementioned NMC 811 half cells, it is clear that the cause of reduced capacity is a progressive increase in total polarization (Figures 2a–d). We believe this behavior is due to continual parasitic decomposition of the electrolyte, particularly due to the strong correlation of the overpotential and Coulombic efficiency (CE), with average values of 83.3%, 96.0%, and 98.5% for LiTFSI, LiNFS, and LiNFSI, respectively, over the duration of cycling (Figure 2e). In addition, this progressive decomposition appears to be exacerbated when the conductive carbon content is reduced to 2% (see Figure S2 in the Supporting Information), which indicates that the passivation at the NMC 811/electrolyte interphase dictates this behavior. Such decomposition is likely related to the coupled

destabilization effect of anions on their local solvent environment, which will be further discussed below.³² Of note, the CF_3 radicals formed during TFSI, and likely OTF decomposition are known to be highly reactive and easily formed.³³ We also find that these stability trends extend to the Li metal anode, where the LiNFSI DME electrolyte was found to be slightly improved to that of LiTFSI (see Figure S3a in the Supporting Information). However, it is noteworthy that, like TFSI, the LiNFSI electrolyte must be coupled with LiNO_3 in order to ensure stable Li metal cycling (Figure S3b in the Supporting Information).

The modification of each anion may result in either an intrinsic thermodynamic stabilization of the HOMO states found within the system, which defines the intrinsic oxidative stability, or the formation of a passivating CEI as a result of anion decomposition. Thermodynamic (i.e., intrinsic) stabilization of the electrolyte is typically induced through either the alteration of the ion solvation structure, or the intrinsic

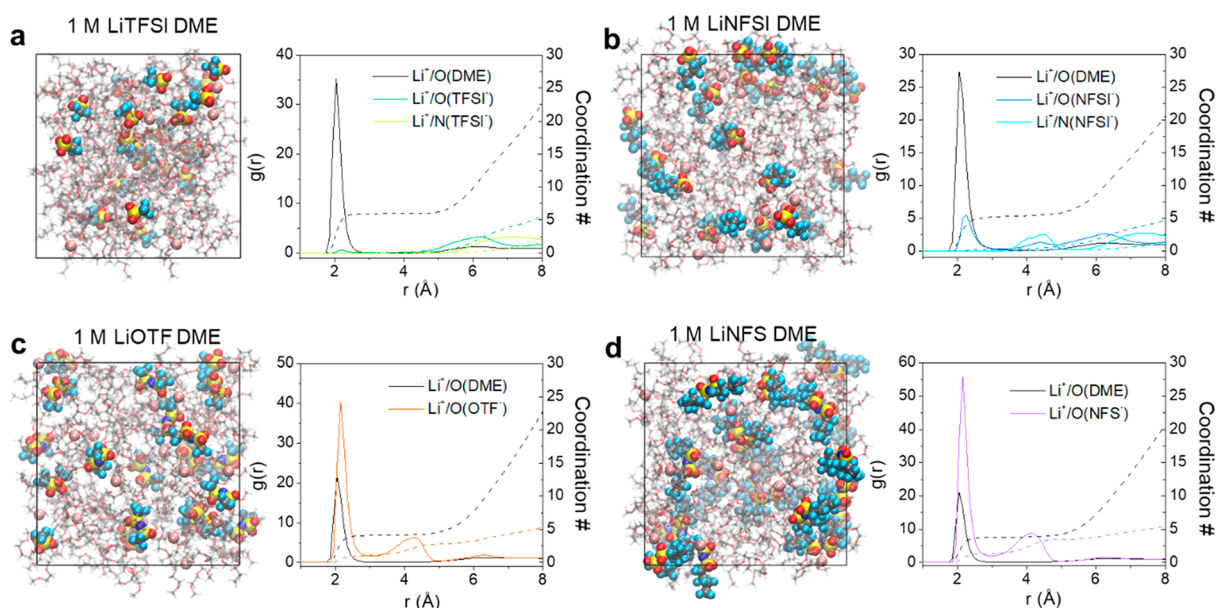


Figure 3. Molecular dynamics simulations. Simulation snapshot and Li^+ radial distribution functions of (a) 1 M LiTFSI DME, (b) 1 M LiNFSI DME, (c) 1 M LiOTF DME, and (d) 1 M LiNFS DME.

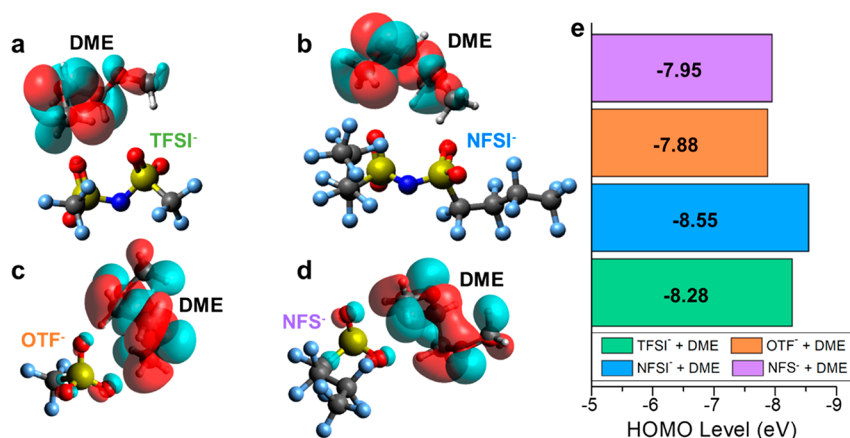


Figure 4. Density functional theory simulations of anion/DME pairs. Visualized HOMO orbitals of (a) $\text{TFSI}^- + \text{DME}$, (b) $\text{NFSI}^- + \text{DME}$, (c) $\text{OTF}^- + \text{DME}$, and (d) $\text{NFS}^- + \text{DME}$ pairs. Also shown are (e) the HOMO energies of the systems of interest.

stabilization of the HOMO of each individual electrolyte component.^{34,35} Considering the former of these intrinsic stabilization mechanisms, there is relative consensus regarding the stabilizing effect of cation–anion pairs in solution.^{30,36,37} To examine any change in these factors associated with anion modification, the solvation structures were explored via molecular dynamics (MD) simulations of the 1 M solutions, as described in the Supporting Information and Table S1.

The MD simulations are shown in Figure 3, where the solvation structures of each electrolyte are displayed through the Li^+ radial distribution function averaged over 5 ns of production dynamics. When examining the effect of chain length on the preferred structure of the sulfonylimide anions, it is observed that the 1 M LiTFSI DME system heavily prefers a solvent coordinated electrolyte, where the average Li^+ solvation shell was found to be $\text{Li}^+(\text{DME})_{3.0}(\text{TFSI}^-)_{0.1}$ (Figure 3a). When the chain length was increased to NFSI, a small increase in probability of NFSI[−] coordination was observed; however, it is crucial to note that its effect on average structure is relatively low, where an average structure of $\text{Li}^+(\text{DME})_{2.7}(\text{NFSI}^-)_{0.2}$ was

predicted (Figure 3b). This trend was found to be replicated by the sulfonate series, where the average structure of $\text{Li}^+(\text{DME})_{2.0}(\text{OTF}^-)_{1.0}$ (Figure 3c), and $\text{Li}^+(\text{DME})_{1.9}(\text{NFS}^-)_{1.3}$. Given that there is a negligible effect of anion C_xF_y group length on the solvation structure of the electrolyte, we believe that the thermodynamic stabilization of the system via this route is unlikely.

To address a possible intrinsic stabilization route for the electrochemical trends previously discussed, density functional theory (DFT) calculations were performed on electrolyte components of interest. Previous theoretical works have concluded that the oxidative stability of battery electrolytes is best assessed in cells containing anion/solvent pairs instead of individual components, because of the destabilizing effect of electronic interactions between them, which we have also applied here.^{32,38} As shown in Figures 4a–d, it was found that the highest occupied molecular orbital (HOMO) was localized almost entirely to DME, regardless of the anion, despite the high stability of DME predicted by DFT optimization of single

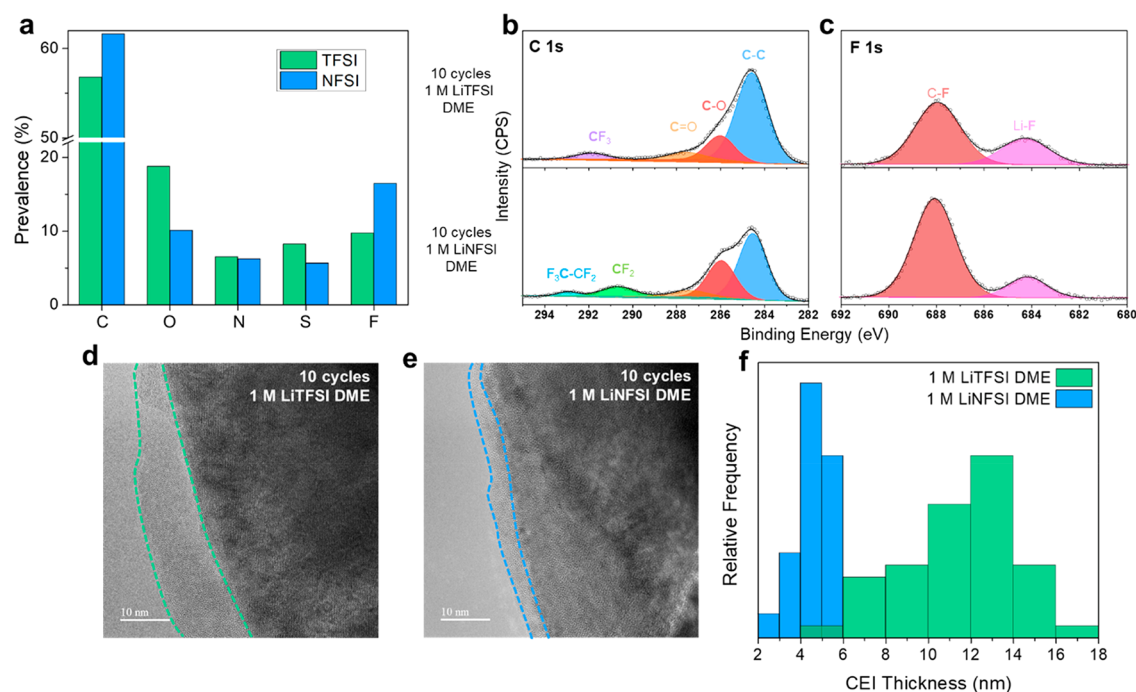


Figure 5. X-ray photoelectron spectroscopy of NMC 811 electrodes employing a PAN binder. (a) Atomic prevalence of CEI components of interest. (b, c) Fitted C 1s (panel (b)), and F 1s spectra (panel (c)) of the samples of interest. Cryogenic TEM micrograph of the CEI formed on NMC 811 electrodes after 10 cycles in (d) 1 M LiTFSI DME and (e) 1 M LiNFSI DME. CEI boundaries are highlighted with dotted lines. (f) Statistical distribution of CEI thickness.

components in vacuum (see Table S2 in the Supporting Information).

These results indicate that, in the electrolytes of interest, DME would preferentially decompose at the interphase, likely involving deprotonation of the solvent.⁴⁰ Such a phenomenon is typically considered to be a highly undesirable outcome, because of the possibility of gas generation,^{39,41} and therefore describes the progressive decomposition observed in half cell tests. It is important to note that this does not preclude anion decomposition induced by further interactions between generated radicals and/or an increased local concentration of anions due at the positively charged interphase. Although a modest stabilization effect was observed in conjunction with C_xF_y lengthening (Figure 4e), we reason by analogy that the 0.07 eV difference between NFS^- and OTF^- does not describe their vastly varied oxidative performance, nor does the DFT predicted $OTF^- < NFS^- < TFSI^- < NFSI^-$ match the experimental trend ($OTF^- < TFSI^- < NFS^- < NFSI^-$).

From MD and DFT simulations, we conclude that an intrinsic stabilization of the electrolyte via anion modification is unlikely. This instead implies that the oxidative stability produced by LiNFS and LiNFSI electrolytes is due to the formation of a passivating CEI, which is rarely observed in dilute electrolytes.^{14,15,31,42} To probe the formation of such an interphase, X-ray photoelectron spectroscopy (XPS) was performed on NMC 811 cathodes cycled in 1 M LiTFSI and 1 M LiNFSI DME 10 times. The sulfonate moiety was not considered in such analysis, because of the inability of 1 M LiOTF to provide viable cycles (Figure 2c). It is crucial to note that the NMC 811 electrodes prepared for XPS utilized a poly(acrylonitrile) (PAN) binder instead of the commonplace poly(vinylene difluoride) (PVDF) to ensure that the fluorine signals observed originated from anion decomposition.

The full XPS spectra of these samples is shown in Figure S5a in the Supporting Information, where a number of trends are readily apparent between the NMC 811 electrodes cycled in 1 M LiTFSI DME and 1 M LiNFSI DME. Of note, it was observed that fluorine was significantly more prevalent in the NFSI-cycled system than that of TFSI, which is generally thought to be an advantageous feature of interphases.³¹ In addition, the oxygen content within the interphase was found to be substantially higher in the case of the TFSI-cycled electrode in a manner disproportionate to the sulfur content, indicating excessive decomposition of solvent, as previously predicted by DFT (Figure 4). The quantitative atomic prevalence trends are shown in Figure 5a, where the interphases formed by 1 M LiTFSI and 1 M LiNFSI DME electrolytes were found to be 9.72% and 16.4% for F and 18.8% and 10.1% for O, respectively.

To investigate the speciation of the regions of interest, the C 1s, F 1s, and O 1s fitted spectra are presented in Figures 5b and 5c, as well as Figure S5b in the Supporting Information. Although the C–C, C–O, and C=O carbon species observed may be attributed to the PAN binder and/or conductive carbon additives within the composite electrode, note that both the CF_3-CF_2 and CF_2 species were identified in the interphase formed by 1 M LiNFSI DME. This implies that salt decomposition on the surface was primarily driven by the SO_2-N-SO_2 portion of the anion, C_4F_9 chains remaining intact on the surface. This decomposition route is also supported by HOMO visualization from DFT simulations of individual anions in vacuum (see Figure S4 in the Supporting Information). The prevalence of these perfluoroalkane species within the CEI formed by 1 M LiNFSI DME was also supported by the F 1s spectra, which indicates that the F signal is dominated by C–F species, whereas the CEI formed in 1 M LiTFSI DME is more balanced between C–F and Li–F,

possibly due to the reactive nature of CF_3 radicals. Lastly, the O 1s spectra of both samples revealed a significantly increased prevalence of R–O–Li and C=O in the interphase formed by 1 M LiTFSI DME, which once again supports the solvent decomposition model proposed previously.

These results indicate that oxidative salt decomposition in the C_4F_9 anion electrolytes results in fluorinated interphases composed largely of fluoroalkanes, which results in passivation toward runaway solvent decomposition during cycling. Our previous results have indicated also that organic fluorine species are beneficial for high voltage cathode cycling,⁴³ which may be due to the solvophobic nature of these groups, as previously proposed in a work employing perfluorinated compounds.⁴⁴ This work suggests that perfluoroalkyl moieties may be a beneficial feature of anions for electrolyte engineering purposes, which prompts further work in the synthesis of these compounds. In addition, lithium salts of increased fluoroalkane length within the bis(C_xF_y sulfonyl)imide and C_xF_y sulfonate anion families, or revisiting fluoroalkyl phosphate salts may also be promising directions.⁴⁵

As a final confirmation of role of the fluorinated interphases in passivation toward solvent decomposition, cryogenic transmission electron microscopy (cryo-TEM) was performed on NMC 811 electrodes cycled 10 times in 1 M LiTFSI and LiNFSI, which reduce beam damages of the CEI at the liquid nitrogen temperature. As shown in Figure 5d, the CEI produced by 1 M LiTFSI DME was found to be significantly thicker than that produced by 1 M LiNFSI DME (Figure 5e). The thickness of these CEIs were measured quantitatively (see the Supporting Information), where it was found that the values exhibited a Gaussian-like distribution centered at ~ 5 and 13 nm for 1 M LiNFSI and 1 M LiTFSI DME samples, respectively (Figure 5f). The progressive growth of these interphases is likely the cause of the increased polarization during cycling (see Figures 2a and 2b), where the LiNFSI interphase grows at a much slower rate. These results substantiate the CEI stabilization mechanism proposed previously, and they quantify an otherwise qualitative phenomenon.

In this work, we have demonstrated an improvement in oxidative stability of low-cost, dilute nonfluorinated ether electrolytes via anion modification. Specifically, by increasing the anion perfluoro chain length of LiTFSI and LiOTF (terminated by CF_3 groups) to LiNFSI and LiNFS (terminated by C_4F_9 groups), it was found that the oxidative stability could be improved such that NMC 811 cathodes could be reversibly cycled up to 4.4 V vs Li/Li⁺. Through MD and DFT calculations, it was determined that these anion modifications did not result in meaningful changes in the solvation structure, HOMO levels, or likely decomposition paths present in the electrolytes, thus rendering an intrinsic stabilization mechanism unlikely. Instead, the stabilization route was concluded to be a result of the fluorinated CEI formed by these anions. This work provides a potential route forward for the application low-cost ether electrolytes in Li metal batteries.

■ ASSOCIATED CONTENT

SI Supporting Information

The Supporting Information is available free of charge at <https://pubs.acs.org/doi/10.1021/acseenergylett.1c02723>.

Experimental and computational methods, linear voltammetry of electrolyte on stainless-steel current

collectors, galvanostatic cycling of NMC 811 electrodes at increased active mass ratio, Li metal Coulombic efficiency measurements, MD simulation details, additional DFT data (PDF)

■ AUTHOR INFORMATION

Corresponding Author

Ping Liu – Department of NanoEngineering, Program of Materials Science, Program of Chemical Engineering, and Sustainable Power and Energy Center, University of California, San Diego, La Jolla, California 92093, United States; orcid.org/0000-0002-1488-1668; Email: piliu@eng.ucsd.edu

Authors

John Holoubek – Department of NanoEngineering, University of California, San Diego, La Jolla, California 92093, United States; orcid.org/0000-0003-0015-4512

Qizhang Yan – Department of NanoEngineering, University of California, San Diego, La Jolla, California 92093, United States

Haodong Liu – Department of NanoEngineering, University of California, San Diego, La Jolla, California 92093, United States

Emma J. Hopkins – Program of Materials Science, University of California, San Diego, La Jolla, California 92093, United States

Zhaohui Wu – Program of Chemical Engineering, University of California, San Diego, La Jolla, California 92093, United States

Sicen Yu – Program of Materials Science, University of California, San Diego, La Jolla, California 92093, United States

Jian Luo – Department of NanoEngineering, Program of Materials Science, Program of Chemical Engineering, and Sustainable Power and Energy Center, University of California, San Diego, La Jolla, California 92093, United States

Tod A. Pascal – Department of NanoEngineering, Program of Chemical Engineering, and Sustainable Power and Energy Center, University of California, San Diego, La Jolla, California 92093, United States; orcid.org/0000-0003-2096-1143

Zheng Chen – Department of NanoEngineering, Program of Materials Science, Program of Chemical Engineering, and Sustainable Power and Energy Center, University of California, San Diego, La Jolla, California 92093, United States; orcid.org/0000-0002-9186-4298

Complete contact information is available at: <https://pubs.acs.org/10.1021/acseenergylett.1c02723>

Author Contributions

J.H. and P.L. conceived the original idea. P.L. directed the project. J.H., Q.Y., and H.L. performed the experiments. Q.Y., E.H., Z.W., and S.Y. assisted with characterization. J.H., E.H., and P.L. wrote the paper. All authors discussed the results and commented on the manuscript.

Notes

The authors declare no competing financial interest.

ACKNOWLEDGMENTS

This work was supported by a NASA Space Technology Graduate Research Opportunity. This work was also partially supported by the Office of Vehicle Technologies of the U.S. Department of Energy through the Advanced Battery Materials Research (BMR) Program (Battery500 Consortium), under Contract No. DE-EE0007764 to P.L., Q.Y. and J.L. acknowledge the support of the Center for Synthetic Control Across Length-scales for Advancing Rechargeables (SCALAR), an Energy Frontier Research Center funded by the United States Department of Energy, Office of Science, Basic Energy Sciences, under Award No. DESC0019381, for the microscopy and interface characterization. Part of the work used the UCSD-MTI Battery Fabrication Facility and the UCSD-Arbin Battery Testing Facility. SEM characterization was performed at the San Diego Nanotechnology Infrastructure (SDNI) of UCSD, a member of the National Nanotechnology Coordinated Infrastructure, which is supported by the National Science Foundation (Grant No. ECCS-1542148). TEM experiments were conducted using the facilities in the Irvine Materials Research Institute (IMRI), which is supported in part by the National Science Foundation through the UC Irvine Materials Research Science and Engineering Center (No. DMR-2011967). This work also used the Extreme Science and Engineering Discovery Environment (XSEDE)⁴⁶ on the Expanse supercomputer at the San Diego Supercomputing Center, which is supported by the National Science Foundation (Grant No. ACI-1548562).

REFERENCES

- (1) Liu, J.; Bao, Z.; Cui, Y.; Dufek, E. J.; Goodenough, J. B.; Khalifah, P.; Li, Q.; Liaw, B. Y.; Liu, P.; Manthiram, A.; Meng, Y. S.; Subramanian, V. R.; Toney, M. F.; Viswanathan, V. V.; Whittingham, M. S.; Xiao, J.; Xu, W.; Yang, J.; Yang, X.-Q.; Zhang, J.-G. Pathways for Practical High-Energy Long-Cycling Lithium Metal Batteries. *Nat. Energy* **2019**, *4* (3), 180–186.
- (2) Xu, K. Electrolytes and Interphases in Li-Ion Batteries and Beyond. *Chem. Rev.* **2014**, *114* (23), 11503–11618.
- (3) Winter, M.; Barnett, B.; Xu, K. Before Li Ion Batteries. *Chem. Rev.* **2018**, *118* (23), 11433–11456.
- (4) Xu, W.; Wang, J.; Ding, F.; Chen, X.; Nasybulin, E.; Zhang, Y.; Zhang, J.-G. Lithium Metal Anodes for Rechargeable Batteries. *Energy Environ. Sci.* **2014**, *7* (2), 513–537.
- (5) Lin, D.; Liu, Y.; Cui, Y. Reviving the Lithium Metal Anode for High-Energy Batteries. *Nat. Nanotechnol.* **2017**, *12* (3), 194–206.
- (6) Li, S.; Jiang, M.; Xie, Y.; Xu, H.; Jia, J.; Li, J. Developing High-Performance Lithium Metal Anode in Liquid Electrolytes: Challenges and Progress. *Adv. Mater.* **2018**, *30* (17), 1706375.
- (7) Qian, J.; Henderson, W. A.; Xu, W.; Bhattacharya, P.; Engelhard, M.; Borodin, O.; Zhang, J.-G. High Rate and Stable Cycling of Lithium Metal Anode. *Nat. Commun.* **2015**, *6* (1), 1–9.
- (8) Niu, C.; Lee, H.; Chen, S.; Li, Q.; Du, J.; Xu, W.; Zhang, J.-G.; Whittingham, M. S.; Xiao, J.; Liu, J. High-Energy Lithium Metal Pouch Cells with Limited Anode Swelling and Long Stable Cycles. *Nat. Energy* **2019**, *4* (7), 551–559.
- (9) Alvarado, J.; Schroeder, M. A.; Pollard, T. P.; Wang, X.; Lee, J. Z.; Zhang, M.; Wynn, T.; Ding, M.; Borodin, O.; Meng, Y. S.; Xu, K. Bisalt Ether Electrolytes: A Pathway towards Lithium Metal Batteries with Ni-Rich Cathodes. *Energy Environ. Sci.* **2019**, *12* (2), 780–794.
- (10) Yu, Z.; Wang, H.; Kong, X.; Huang, W.; Tsao, Y.; Mackanic, D. G.; Wang, K.; Wang, X.; Huang, W.; Choudhury, S.; Zheng, Y.; Amanchukwu, C. V.; Hung, S. T.; Ma, Y.; Lomeli, E. G.; Qin, J.; Cui, Y.; Bao, Z. Molecular Design for Electrolyte Solvents Enabling Energy-Dense and Long-Cycling Lithium Metal Batteries. *Nat. Energy* **2020**, *5* (7), 526–533.
- (11) Zhang, X.-Q.; Chen, X.; Hou, L.-P.; Li, B.-Q.; Cheng, X.-B.; Huang, J.-Q.; Zhang, Q. Regulating Anions in the Solvation Sheath of Lithium Ions for Stable Lithium Metal Batteries. *ACS Energy Lett.* **2019**, *4* (2), 411–416.
- (12) Ren, X.; Zou, L.; Cao, X.; Engelhard, M. H.; Liu, W.; Burton, S. D.; Lee, H.; Niu, C.; Matthews, B. E.; Zhu, Z.; Wang, C.; Arey, B. W.; Xiao, J.; Liu, J.; Zhang, J.-G.; Xu, W. Enabling High-Voltage Lithium-Metal Batteries under Practical Conditions. *Joule* **2019**, *3* (7), 1662–1676.
- (13) Yoshida, K.; Nakamura, M.; Kazue, Y.; Tachikawa, N.; Tsuzuki, S.; Seki, S.; Dokko, K.; Watanabe, M. Oxidative-Stability Enhancement and Charge Transport Mechanism in Glyme–Lithium Salt Equimolar Complexes. *J. Am. Chem. Soc.* **2011**, *133* (33), 13121–13129.
- (14) Ren, X.; Zou, L.; Jiao, S.; Mei, D.; Engelhard, M. H.; Li, Q.; Lee, H.; Niu, C.; Adams, B. D.; Wang, C.; Liu, J.; Zhang, J.-G.; Xu, W. High-Concentration Ether Electrolytes for Stable High-Voltage Lithium Metal Batteries. *ACS Energy Lett.* **2019**, *4* (4), 896–902.
- (15) Jiao, S.; Ren, X.; Cao, R.; Engelhard, M. H.; Liu, Y.; Hu, D.; Mei, D.; Zheng, J.; Zhao, W.; Li, Q.; Liu, N.; Adams, B. D.; Ma, C.; Liu, J.; Zhang, J.-G.; Xu, W. Stable Cycling of High-Voltage Lithium Metal Batteries in Ether Electrolytes. *Nat. Energy* **2018**, *3* (9), 739.
- (16) Niu, C.; Liu, D.; Lochala, J. A.; Anderson, C. S.; Cao, X.; Gross, M. E.; Xu, W.; Zhang, J.-G.; Whittingham, M. S.; Xiao, J.; Liu, J. Balancing Interfacial Reactions to Achieve Long Cycle Life in High-Energy Lithium Metal Batteries. *Nat. Energy* **2021**, *6* (7), 723–732.
- (17) Weber, R.; Genovese, M.; Louli, A. J.; Hames, S.; Martin, C.; Hill, I. G.; Dahn, J. R. Long Cycle Life and Dendrite-Free Lithium Morphology in Anode-Free Lithium Pouch Cells Enabled by a Dual-Salt Liquid Electrolyte. *Nat. Energy* **2019**, *4* (8), 683–689.
- (18) Louli, A. J.; Eldesoky, A.; Weber, R.; Genovese, M.; Coon, M.; deGooyer, J.; Deng, Z.; White, R. T.; Lee, J.; Rodgers, T.; Petibon, R.; Hy, S.; Cheng, S. J. H.; Dahn, J. R. Diagnosing and Correcting Anode-Free Cell Failure via Electrolyte and Morphological Analysis. *Nat. Energy* **2020**, *5*, 693–702.
- (19) Markevich, E.; Salitra, G.; Chesneau, F.; Schmidt, M.; Aurbach, D. Very Stable Lithium Metal Stripping–Plating at a High Rate and High Areal Capacity in Fluoroethylene Carbonate-Based Organic Electrolyte Solution. *ACS Energy Lett.* **2017**, *2* (6), 1321–1326.
- (20) Liu, Y.; Lin, D.; Li, Y.; Chen, G.; Pei, A.; Nix, O.; Li, Y.; Cui, Y. Solubility-Mediated Sustained Release Enabling Nitrate Additive in Carbonate Electrolytes for Stable Lithium Metal Anode. *Nat. Commun.* **2018**, *9* (1), 3656.
- (21) Niu, C.; Pan, H.; Xu, W.; Xiao, J.; Zhang, J.-G.; Luo, L.; Wang, C.; Mei, D.; Meng, J.; Wang, X.; Liu, Z.; Mai, L.; Liu, J. Self-Smoothing Anode for Achieving High-Energy Lithium Metal Batteries under Realistic Conditions. *Nat. Nanotechnol.* **2019**, *14* (6), 594–601.
- (22) Liu, H.; Yue, X.; Xing, X.; Yan, Q.; Huang, J.; Petrova, V.; Zhou, H.; Liu, P. A Scalable 3D Lithium Metal Anode. *Energy Storage Mater.* **2019**, *16*, 505–511.
- (23) Lopez, J.; Pei, A.; Oh, J. Y.; Wang, G.-J. N.; Cui, Y.; Bao, Z. Effects of Polymer Coatings on Electrodeposited Lithium Metal. *J. Am. Chem. Soc.* **2018**, *140* (37), 11735–11744.
- (24) Zhou, H.; Yu, S.; Liu, H.; Liu, P. Protective Coatings for Lithium Metal Anodes: Recent Progress and Future Perspectives. *J. Power Sources* **2020**, *450*, 227632.
- (25) Kim, J.; Lee, D.-J.; Jung, H.-G.; Sun, Y.-K.; Hassoun, J.; Scrosati, B. An Advanced Lithium-Sulfur Battery. *Adv. Funct. Mater.* **2013**, *23* (8), 1076–1080.
- (26) Agostini, M.; Xiong, S.; Matic, A.; Hassoun, J. Polysulfide-Containing Glyme-Based Electrolytes for Lithium Sulfur Battery. *Chem. Mater.* **2015**, *27* (13), 4604–4611.
- (27) Gupta, A.; Bhargava, A.; Jones, J.-P.; Bugga, R. V.; Manthiram, A. Influence of Lithium Polysulfide Clustering on the Kinetics of Electrochemical Conversion in Lithium–Sulfur Batteries. *Chem. Mater.* **2020**, *32* (5), 2070–2077.
- (28) Suo, L.; Hu, Y.-S.; Li, H.; Armand, M.; Chen, L. A New Class of Solvent-in-Salt Electrolyte for High-Energy Rechargeable Metallic Lithium Batteries. *Nat. Commun.* **2013**, *4*, 1481.

(29) Conte, L.; Gambaretto, G.; Caporiccio, G.; Alessandrini, F.; Passerini, S. Perfluoroalkanesulfonylimides and Their Lithium Salts: Synthesis and Characterisation of Intermediates and Target Compounds. *J. Fluorine Chem.* **2004**, *125* (2), 243–252.

(30) Suo, L.; Borodin, O.; Gao, T.; Olguin, M.; Ho, J.; Fan, X.; Luo, C.; Wang, C.; Xu, K. Water-in-Salt[®] Electrolyte Enables High-Voltage Aqueous Lithium-Ion Chemistries. *Science* **2015**, *350* (6263), 938–943.

(31) Fan, X.; Chen, L.; Borodin, O.; Ji, X.; Chen, J.; Hou, S.; Deng, T.; Zheng, J.; Yang, C.; Liou, S.-C.; Amine, K.; Xu, K.; Wang, C. Non-Flammable Electrolyte Enables Li-Metal Batteries with Aggressive Cathode Chemistries. *Nat. Nanotechnol.* **2018**, *13* (8), 715–722.

(32) Fadel, E. R.; Faglioni, F.; Samsonidze, G.; Molinari, N.; Merinov, B. V.; Goddard, W. A. G., III; Grossman, J. C.; Mailoa, J. P.; Kozinsky, B. Role of Solvent-Anion Charge Transfer in Oxidative Degradation of Battery Electrolytes. *Nat. Commun.* **2019**, *10* (1), 3360.

(33) Qiao, L.; Oteo, U.; Zhang, Y.; Peña, S. R.; Martínez-Ibañez, M.; Santiago, A.; Cid, R.; Meabe, L.; Manzano, H.; Carrasco, J.; Zhang, H.; Armand, M. Trifluoromethyl-Free Anion for Highly Stable Lithium Metal Polymer Batteries. *Energy Storage Mater.* **2020**, *32*, 225–233.

(34) Zhang, Z.; Hu, L.; Wu, H.; Weng, W.; Koh, M.; Redfern, P. C.; Curtiss, L. A.; Amine, K. Fluorinated Electrolytes for 5 V Lithium-Ion Battery Chemistry. *Energy Environ. Sci.* **2013**, *6* (6), 1806–1810.

(35) Borodin, O.; Behl, W.; Jow, T. R. Oxidative Stability and Initial Decomposition Reactions of Carbonate, Sulfone, and Alkyl Phosphate-Based Electrolytes. *J. Phys. Chem. C* **2013**, *117* (17), 8661–8682.

(36) Wang, J.; Yamada, Y.; Sodeyama, K.; Chiang, C. H.; Tateyama, Y.; Yamada, A. Superconcentrated Electrolytes for a High-Voltage Lithium-Ion Battery. *Nat. Commun.* **2016**, *7*, 12032.

(37) Yamada, Y.; Wang, J.; Ko, S.; Watanabe, E.; Yamada, A. Advances and Issues in Developing Salt-Concentrated Battery Electrolytes. *Nat. Energy* **2019**, *4* (4), 269–280.

(38) Kim, D. Y.; Park, M. S.; Lim, Y.; Kang, Y.-S.; Park, J.-H.; Doo, S.-G. Computational Comparison of Oxidation Stability: Solvent/Salt Monomers vs Solvent–Solvent/Salt Pairs. *J. Power Sources* **2015**, *288*, 393–400.

(39) Teng, X.; Zhan, C.; Bai, Y.; Ma, L.; Liu, Q.; Wu, C.; Wu, F.; Yang, Y.; Lu, J.; Amine, K. In Situ Analysis of Gas Generation in Lithium-Ion Batteries with Different Carbonate-Based Electrolytes. *ACS Appl. Mater. Interfaces* **2015**, *7* (41), 22751–22755.

(40) Borodin, O.; Behl, W.; Jow, T. R. Oxidative Stability and Initial Decomposition Reactions of Carbonate, Sulfone, and Alkyl Phosphate-Based Electrolytes. *J. Phys. Chem. C* **2013**, *117* (17), 8661–8682.

(41) Galushkin, N. E.; Yazvinskaya, N. N.; Galushkin, D. N. Mechanism of Gases Generation during Lithium-Ion Batteries Cycling. *J. Electrochem. Soc.* **2019**, *166* (6), A897.

(42) Fan, X.; Chen, L.; Ji, X.; Deng, T.; Hou, S.; Chen, J.; Zheng, J.; Wang, F.; Jiang, J.; Xu, K.; Wang, C. Highly Fluorinated Interphases Enable High-Voltage Li-Metal Batteries. *Chem.* **2018**, *4* (1), 174–185.

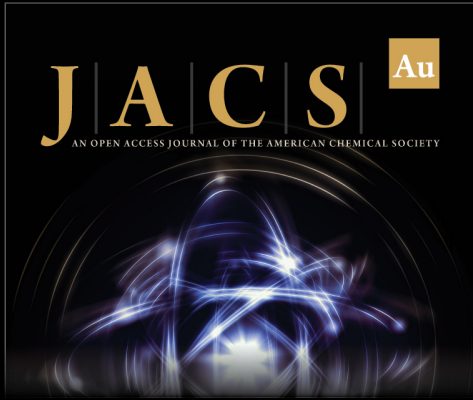
(43) Holoubek, J.; Yu, M.; Yu, S.; Li, M.; Wu, Z.; Xia, D.; Bhaladhare, P.; Gonzalez, M. S.; Pascal, T. A.; Liu, P.; Chen, Z. An All-Fluorinated Ester Electrolyte for Stable High-Voltage Li Metal Batteries Capable of Ultra-Low-Temperature Operation. *ACS Energy Lett.* **2020**, *5*, 1438–1447.

(44) Zhu, Y.; Casselman, M. D.; Li, Y.; Wei, A.; Abraham, D. P. Perfluoroalkyl-Substituted Ethylene Carbonates: Novel Electrolyte Additives for High-Voltage Lithium-Ion Batteries. *J. Power Sources* **2014**, *246*, 184–191.

(45) Schmidt, M.; Heider, U.; Kuehner, A.; Oesten, R.; Jungnitz, M.; Ignat'ev, N.; Sartori, P. Lithium Fluoroalkylphosphates: A New Class of Conducting Salts for Electrolytes for High Energy Lithium-Ion Batteries. *J. Power Sources* **2001**, *97–98*, 557–560.


(46) Towns, J.; Cockerill, T.; Dahan, M.; Foster, I.; Gauthier, K.; Grimshaw, A.; Hazlewood, V.; Lathrop, S.; Lifka, D.; Peterson, G. D.;


Roskies, R.; Scott, J. R.; Wilkins-Diehr, N. XSEDE: Accelerating Scientific Discovery. *Comput. Sci. Eng.* **2014**, *16* (5), 62–74.



JACS Au
AN OPEN ACCESS JOURNAL OF THE AMERICAN CHEMICAL SOCIETY

Editor-in-Chief
Prof. Christopher W. Jones
Georgia Institute of Technology, USA

Open for Submissions 

pubs.acs.org/jacsau  ACS Publications
Most Trusted. Most Cited. Most Read.